Gas-Phase Chemistry

DOI: 10.1002/ange.201208958

# IR Spectrum and Structure of a Protonated Disilane: Probing the Si–H–Si Proton Bridge**

*Marco Savoca, Judith Langer, and Otto Dopfer**

Although carbon and silicon are both group IV elements, their chemical bonding behavior is rather different. As Si–Si and Si–H bonds are weaker and less directional than C–C and C–H bonds, the bonding motifs in $Si_nH_m$ show a much larger variety than their $C_nH_m$ analogs. $Si_nH_m$ often exhibit stable Si–H–Si bridges, which are rare for $C_nH_m$. In contrast to $C_nH_m^{(\pm)}$, $Si_nH_m^{(\pm)}$ are far less well-characterized because of the lack of suitable precursors. For example, although few $SiH_m^+$ ions were studied by IR spectroscopy,[1] no spectroscopic data are available for $Si_nH_m^+$ with $n>1$. In addition to theory of chemical bonding, $Si_nH_m$ are interesting from a materials science point of view, as H passivation at the surface is predicted to turn reactive bare $Si_n$ clusters into stable novel nanostructures with potential for technological applications.[2] $Si_nH_m^{(\pm)}$ spectra are also required for comparison with astronomical data[3] and diagnostics of silane plasmas used in the fabrication of microelectronic silicon-based devices.[4] Here, we report the IR spectrum of disilanium, $Si_2H_7^+$, a fully H-passivated $Si_2$ core with a Si–H–Si bridge described by a three-center two-electron (3c-2e) bond (Figure 1).

Almost no information is available for the $Si_2H_7^+$ cation. Early MP2/6-31G* calculations[5] predict a $D_{3d}$ symmetric global minimum with a linear $H_3Si{-}H{-}SiH_3$ proton bridge and a weakly bound $Si_2H_5^+{\cdot}H_2$ complex as local minimum, with stabilization energies of $D_0=146$ and about 38 kJ mol$^{-1}$, respectively. The $Si_2H_7^+$ cation dissociates barrierless into $SiH_3^+ + SiH_4$ with a measured binding energy greater than 146 kJ mol$^{-1}$.[6] Binding of further $SiH_4$ ligands to $SiH_3^+$ is much weaker ($<40$ kJ mol$^{-1}$), suggesting that $Si_2H_7^+$ forms a stable core in $SiH_3^+{\cdot}(SiH_4)_n$ clusters.[6] Although dissociation into $Si_2H_5^+ + H_2$ is less endothermic than into $SiH_3^+ + SiH_4$, it involves a high barrier lying slightly above the $SiH_3^+ + SiH_4$ limit.[5,6]

The IR spectrum of $Si_2H_7^+$ is obtained by Ne-tagging IR photodissociation (IRPD) spectroscopy,[7] a sensitive approach recently used to elucidate the structures of simple $C_xH_y^+$ ions[8] and $Si_2H_6^+$.[9] $Si_2H_7^+{\cdot}Ne$ ions are generated in a supersonic plasma expansion containing $SiH_4$ and Ne. Due to the small $Si_2H_7^+{\cdot}Ne$ binding energy ($<3$ kJ mol$^{-1}$), the influence of Ne on the $Si_2H_7^+$ spectrum is negligible, and the single-photon IRPD spectrum of $Si_2H_7^+{\cdot}Ne$ (Figure 2) provides a close approximation to the IR spectrum of $Si_2H_7^+$. All bands (A–E) in the 650–2200 cm$^{-1}$ range are assigned to fundamentals of the bridged $H_3Si{-}H{-}SiH_3$ ion.

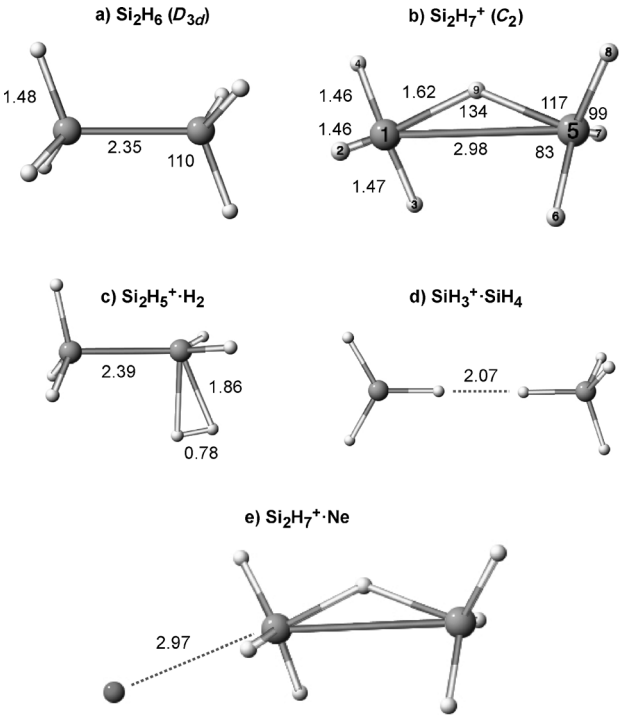


***Figure 1.*** Structures of a) $Si_2H_6$ ($D_{3d}$), b) $Si_2H_7^+$ ($C_2$, with atom numbering), c) $Si_2H_5^+{\cdot}H_2$, d) $SiH_3^+{\cdot}SiH_4$, and e) $Si_2H_7^+{\cdot}Ne$ calculated at the MP2/aug-cc-pVTZ level. Relevant structural parameters are given in ångströms and degrees (Table S1).

MP2/aug-cc-pVTZ calculations elucidate the energetic, structural, electronic, and vibrational properties of $Si_2H_6$, $Si_2H_7^+$, and $Si_2H_7^+{\cdot}Ne$. The most stable structure of $Si_2H_7^+$ has a bent 3c-2e Si–H–Si bridge (Figure 1b). In contrast to all previous calculations at the MP2/6-31G* or lower levels,[5] it has $C_2$ rather than $D_{3d}$ symmetry. This structure can be generated either by protonation of the Si–Si single bond of $Si_2H_6$ or by addition of $SiH_4$ to $SiH_3^+$. In the latter case, $SiH_4$ binds to the vacant electrophilic $3p_z$ orbital of $SiH_3^+$ in an orientation that allows for a weak Si–Si contact. Protonation of $Si_2H_6$ causes a drastic elongation of the Si–Si bond from 2.35 to 2.98 Å. The bent Si–H–Si bridge (134°) has long Si–H bonds (1.62 Å). The Si–H bonds of the $SiH_3$ groups contract upon protonation from 1.481 to about 1.465 Å, which is between those in $SiH_3^+$ (1.462 Å) and $SiH_4$ (1.478 Å). All

[*] Dipl.-Phys. M. Savoca, Dr. J. Langer, Prof. Dr. O. Dopfer
Institut für Optik und Atomare Physik
Technische Universität Berlin
Hardenbergstr. 36, 10623 Berlin (Germany)
E-mail: dopfer@physik.tu-berlin.de

[**] This study was supported by the Deutsche Forschungsgemeinschaft (grant numbers DO 729/5 and FOR 1282).

Supporting information for this article is available on the WWW under http://dx.doi.org/10.1002/anie.201208958.

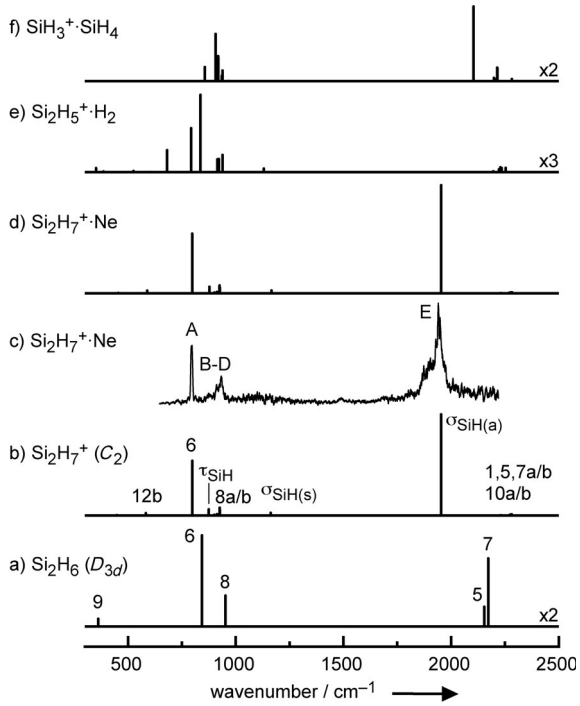


***Figure 2.*** Experimental IRPD spectrum of c) $Si_2H_7^+ \cdot Ne$ compared to the linear stick IR absorption spectra of a) $Si_2H_6$ ($D_{3d}$), b) $Si_2H_7^+$ ($C_2$), d) $Si_2H_7^+ \cdot Ne$, e) $Si_2H_5^+ \cdot H_2$, and f) $SiH_3^+ \cdot SiH_4$ in their ground electronic states calculated at the MP2/aug-cc-pVTZ level (Figure 1). The positions and assignments of the observed transitions are listed in Table S2.

SiSiH bond angles deviate largely from the tetrahedral configuration in $Si_2H_6$.

The natural bond orbital (NBO) charge distribution provides insight into the nature of the 3c-2e bond in $Si_2H_7^+$ (Figure 3). The charges $q_{Si} = 0.6$ and $q_H = -0.2$ e in $Si_2H_6$ are

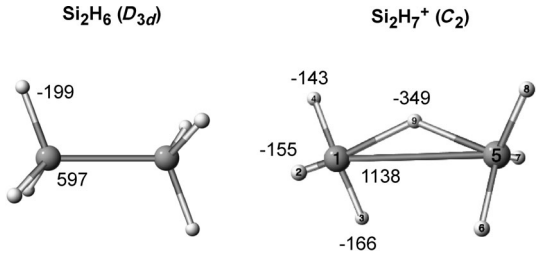


***Figure 3.*** NBO charge distribution (in me) of $Si_2H_6$ ($D_{3d}$) and $Si_2H_7^+$ ($C_2$) evaluated at the MP2/aug-cc-pVTZ level.

consistent with the higher electronegativity of H than Si. In $Si_2H_7^+$, both Si atoms absorb the excess positive charge ($q_{Si} = +1.14$ e), whereas all H atoms remain negative ($-q_H = 0.14$-$0.35$ e). Each $SiH_3$ unit in $Si_2H_7^+$ carries $+0.67$ e, that is, $SiH_4$ transfers formally 0.34 e into the $3p_z$ orbital of $SiH_3^+$. In the limit of ionic bonding, $Si_2H_7^+$ can be described as $H_3Si^+ \cdots H^- \cdots SiH_3^+$. Hence, $Si_2H_7^+$ is rather different from $N_2H_7^+$ and $O_2H_5^+$, which in the ionic limit are proton-bound complexes, $H_3N \cdots H^+ \cdots NH_3$ and $H_2O \cdots H^+ \cdots OH_2$.[10] This view of

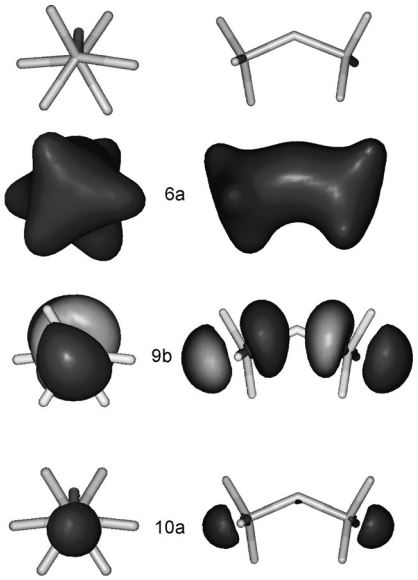


***Figure 4.*** Front and side views of the three molecular orbitals of the 3c-2e bond in $Si_2H_7^+$ ($C_2$). The occupied 6a orbital is the bonding MO, whereas the vacant 9b and 10a orbitals are antibonding MOs.

bonding in $Si_2H_7^+$ is confirmed by the molecular orbitals (MOs) of its $^1A$ ground-state configuration, $[NeNe](6a)^2(6b)^2(7a)^2(8a)^2(7b)^2(9a)^2(8b)^2$. The three MOs of the 3c-2e bond[11] in Figure 4 are the bonding 6a MO, which is delocalized over the whole $Si_2H_7^+$ ion, and the two vacant antibonding 9b and 10a MOs. All other occupied valence MOs are localized on the $SiH_3^+$ fragments and do not contribute to the 3c-2e bond (see Figure S1 in the Supporting Information).

The proton affinity of $Si_2H_6$ has not been measured. The calculated protonation energy for the $C_2$ structure ($E_0 = 745$ kJ mol$^{-1}$) is much larger than that measured for $C_2H_6$ (596 kJ mol$^{-1}$),[12] indicating that protonation of a polysilane Si–Si single bond is more exothermic than protonation of an alkane C–C bond. Collisional activation of $Si_2H_7^+$ produces $SiH_3^+$ as major fragment ion (loss of $SiH_4$, Figure S2). Minor $Si_2H_5^+$ and $Si_2H_3^+$ ions arise from sequential $H_2$ loss. This fragmentation pattern is at first glance surprising, as $H_2$ loss is predicted as lowest fragment channel ($D_0 = 107$ kJ mol$^{-1}$), whereas $SiH_4$ loss requires 148 kJ mol$^{-1}$. The latter value agrees with the lower experimental limit of 146 kJ mol$^{-1}$.[6] The minor observation of $H_2$ loss is due to a barrier higher than the limit for barrierless $SiH_4$ loss.[5]

In addition to the global minimum of $Si_2H_7^+$ ($C_2$), the potential reveals further low-energy stationary points within 5 kJ mol$^{-1}$. These $Si_2H_7^+$ structures with $C_s$, $C_{2v}$, $D_{3d}$, and $D_{3h}$ symmetries (Figure S3 and Tables S3 and S4) are first- or higher-order transition states (TS$n$, $n = 1$–3) for interconversion of equivalent global minima through $SiH_3$ rotation and motion of the central proton around or perpendicular to the Si–Si bond. The $C_s$ ($C_{2v}$) structures at $+0.05$ ($+2.5$) kJ mol$^{-1}$ are TS1 with staggered (eclipsed) geometries with planar H–Si–H–Si–H configurations obtained by rotation of the excess proton and the $SiH_3$ groups around the Si–Si axis (Figure S4). They have similar Si–Si and Si–H bond lengths as

  

the $C_2$ structure. The $D_{3d}$ ($D_{3h}$) structures at +3.7 (+4.3) kJ mol$^{-1}$ are derived from the $C_{2v}$ and $C_s$ structures as TS2 (TS3) by pushing the excess proton in the linear Si–H–Si configuration. They have slightly longer Si–Si distances and the Si–H bonds of the bridge contract substantially. Scrambling of the $SiH_3$ protons in $Si_2H_7^+$ occurs by low internal rotation barriers through the $C_s$ and $C_{2v}$ structures ($V_b <$ 3 kJ mol$^{-1}$), whereas scrambling of the central and terminal protons by a $SiH_3^+ \cdot SiH_4$ transition state ($C_s$) requires much more energy ($V_b = 64$ kJ mol$^{-1}$). Only calculations at the correlated level using extended basis sets properly reproduce the bent Si–H–Si bridge.

In addition to the five low-energy $Si_2H_7^+$ structures with the 3c-2e bond, there are stable high-energy $Si_2H_5^+ \cdot H_2$ and $SiH_3^+ \cdot SiH_4$ complexes on the $Si_2H_7^+$ potential. In $Si_2H_5^+ \cdot H_2$ (Figure 1c), $H_2$ binds weakly to the $3p_z$ orbital of a classical $H_3Si–SiH_2^+$ ion with $D_0 = 41$ kJ mol$^{-1}$. The $SiH_3^+ \cdot SiH_4$ structure in Figure 1d has a weak dihydrogen bond with $D_0 =$ 9.5 kJ mol$^{-1}$, $H_2SiH^+–HSiH_3$, which is typical for X–H–H–Y contacts in which X or Y are more electropositive than H.[13]

To assign the experimental $Si_2H_7^+ \cdot Ne$ spectrum, linear IR absorption spectra are compared for the various $Si_2H_7^+$ minima in Figure 2, namely $Si_2H_7^+$ ($C_2$), $Si_2H_5^+ \cdot H_2$, and $SiH_3^+ \cdot SiH_4$. To judge the effects of protonation and complex formation, calculated IR spectra of $Si_2H_6$, $Si_2H_5^+$, $SiH_3^+$, and $SiH_4$ are presented in Figure 2 and Figure S5. Comparison of the IR spectra of $Si_2H_7^+$ with $C_2$, $C_s$, $C_{2v}$, $D_{3d}$, and $D_{3h}$ symmetries unravels the effects of $SiH_3$ rotation and motion of the central proton on the IR spectrum (Figure S5). All 12 fundamentals of $Si_2H_6$ ($^1A_{1g}$, $D_{3d}$), $\nu_{1–12}$, are known.[14] They transform as $\Gamma_{vib} = 3a_{1g} + a_{1u} + 2a_{2u} + 3e_u + 3e_g$. The $a_{2u}$ ($\nu_{5/6}$) and $e_u$ ($\nu_{7–9}$) modes are IR active. Protonation of $Si_2H_6$ reduces the symmetry from $D_{3d}$ to $C_2$, leading to $\Gamma_{vib} = 11a + 10b$. As a result, all $Si_2H_7^+$ modes become IR active and all e modes split into a/b doublets. The Si–H stretch frequencies of the $SiH_3$ groups ($\nu_{1,5,7,10}$) increase by 68–109 cm$^{-1}$ (3–5%) as a result of the Si–H bond contraction upon protonation and thus shift outside the spectral range investigated. As their IR intensities are reduced by 1–2 orders of magnitude, they would not have been observed in the experimental spectrum at the current sensitivity. The Si–Si stretch frequency ($\nu_3$) decreases by a factor three from 430 to 150 cm$^{-1}$ as a result of proton insertion. The $SiH_3$ torsional frequency ($\nu_4$) decreases slightly from 137 to 119 cm$^{-1}$, in line with a lower barrier for internal rotation calculated for the protonated species (210 vs. 347 cm$^{-1}$).[9] The frequency of the IR-active asymmetric $SiH_3$ deformation decreases by about 27 cm$^{-1}$ and both components ($\nu_{8a,b}$) remain strongly IR active. Similarly, the antisymmetric $SiH_3$ umbrella frequency ($\nu_6$) appears with reduced frequency (−44 cm$^{-1}$) as a prominent transition in the IR spectrum of $Si_2H_7^+$. The frequencies of the degenerate symmetric and antisymmetric $SiH_3$ rocking modes ($\nu_{9,12}$) exhibit large splittings upon protonation (560 and 135 cm$^{-1}$), and their center frequencies are substantially reduced (by 35 and 111 cm$^{-1}$). Due to their low IR intensity, they are not observed in the measured IR spectrum. The excess proton in the Si–H–Si bridge generates three additional fundamentals (Figure S6), and their significant IR intensities provide the fingerprint of the 3c-2e bond. The asymmetric Si–H stretch mode has a rather low frequency because of the long Si–H bonds and dominates the predicted IR spectrum ($\sigma_{SiH(a)} =$ 1954 cm$^{-1}$, $I = 1261$ km mol$^{-1}$). The torsional mode of the proton around the Si–Si bond and the symmetric Si–H stretch mode are predicted with medium IR intensity at $\tau_{SiH} = 875$ and $\sigma_{SiH(s)} = 1163$ cm$^{-1}$. In contrast to all other IR intense modes, $\sigma_{SiH(s)}$ is drastically affected by anharmonicity, which shifts its frequency from 1163 into the 500–700 cm$^{-1}$ range (Figure S7 and Table S5).

To estimate the effects of Ne tagging on the structure and IR spectrum of $Si_2H_7^+$, stable $Si_2H_7^+ \cdot Ne$ complexes have been calculated. In the most stable one (Figure 1e), Ne binds to one of the $SiH_3$ groups with $D_0 = 2.6$ kJ mol$^{-1}$ at a Ne–Si separation of 2.97 Å.[9] The by far largest effects on the $Si_2H_7^+$ geometry upon asymmetric Ne complexation are a slight contraction of the Si–Si bond (1 mÅ) and an asymmetric elongation/contraction of the Si–H bonds in the 3c-2e bond (±3 mÅ). All other bond lengths and angles change less than 1 mÅ and 1°. Except for $\nu_{9b}$, all frequencies are affected by less than 10 cm$^{-1}$ and the IR intensities also show only minor changes. The negligible effects of Ne on the $Si_2H_7^+$ spectrum is not only confirmed by the calculation but also by the similarity of the experimental $Si_2H_7^+ \cdot Ne$ and $Si_2H_7^+ \cdot Ar$ spectra (Figure S8).

Figure 2 reveals a good match between the IRPD spectrum measured for $Si_2H_7^+ \cdot Ne$ and the IR spectra calculated for $Si_2H_7^+ \cdot Ne$ and $Si_2H_7^+$ with $C_2$ symmetry. The bands A–E at 795, 875, 911, 933, and 1941 cm$^{-1}$ are assigned to $\nu_6$, $\tau_{SiH}$, $\nu_{8b}$, $\nu_{8a}$, and $\sigma_{SiH(a)}$, respectively, and the deviation between measured and calculated frequencies is less than 15 cm$^{-1}$. All transitions with predicted intensities $I >$ 50 km mol$^{-1}$ are observed. The measured $Si_2H_7^+ \cdot Ne$ spectrum deviates largely from those predicted for $Si_2H_5^+ \cdot H_2$ and $SiH_3^+ \cdot SiH_4$, confirming that the observed $Si_2H_7^+$ ion has indeed the 3c-2e bond. Bands A–D have widths of about 10 cm$^{-1}$, consistent with unresolved rotational structure. Band E assigned to $\sigma_{SiH(a)}$ exhibits a much larger width of about 120 cm$^{-1}$ and a pronounced substructure. As the $Si_2H_7^+ \cdot Ar$ spectrum shows the same phenomenon, the large width of the $\sigma_{SiH(a)}$ band is attributed to the high fluxionality of the central proton moving in a flat potential perpendicular to the Si–Si axis. Comparison of the IR spectra calculated for the bent and linear structures of $Si_2H_7^+$ (Figure S5) reveals that the $\sigma_{SiH(a)}$ frequency is particularly sensitive to the proton position, confirming that the structure of the $\sigma_{SiH(a)}$ band provides a sensitive probe of the floppy Si–H–Si 3c-2e bond.

In conclusion, Ne-tagging IRPD spectroscopy provides the first spectroscopic and structural characterization of the $Si_2H_7^+$ cation. Analysis of its IR spectrum unravels details of the Si–Si and Si–H bond properties in this fundamental polysilane cation featuring a bent but fluxional 3c-2e bond. The spectrum provides benchmark data for dynamical simulations[15] of the effects of the low-barrier proton and $SiH_3$ motions on the vibrational and electronic properties of this fundamental type of Si–H–Si bond. The combined experimental and quantum chemical approach is suitable for the largely unexplored vibrational and electronic spectroscopy of $Si_nH_m^{\pm}$ ions and their clusters. Future directions

  

include the effects of functional groups, hybrid formation, ligand adsorption, and doping of $Si_nH_m^{\pm}$ with heteroatoms to modify the geometric and electronic properties these fundamental silicon species.

## Experimental Section

IRPD spectra of $Si_2H_7^+$·Ne were recorded in a tandem quadrupole mass spectrometer (QMS1/2).[16] $Si_2H_7^+$·Ne clusters were generated in a pulsed supersonic plasma beam expansion of a $SiH_4$/He/Ne gas mixture (ratio 1:20:300) at 16 bar stagnation pressure. Weakly bound $Si_2H_7^+$·Ne ions were produced by electron and chemical ionization of $SiH_4$ and subsequent three-body aggregation. The composition of $Si_2H_7^+$ and $Si_2H_7^+$·Ne was confirmed by collision-induced dissociation (Figure S2). $Si_2H_7^+$·$^{20}$Ne ions were mass-selected by QMS1 and irradiated in an octopole with a tuneable IR laser pulse ($\nu_{IR}$). Resonant vibrational excitation of $Si_2H_7^+$·Ne induced the rupture of the weak intermolecular bond. Resulting $Si_2H_7^+$ fragments were selected by QMS2 and monitored as a function of $\nu_{IR}$ to obtain IRPD spectra of $Si_2H_7^+$·Ne. The IRPD yield was normalized for laser intensity variations measured with a pyroelectric detector. Calculations were carried out at the MP2/aug-cc-pVTZ level.[17] Relative energies ($E_e$) and binding energies ($D_e$) were corrected for zero-point vibrational energies to derive $E_0$ and $D_0$. Harmonic frequencies are scaled by factors of 0.9518 (0.9742) for frequencies above (below) 1500 $cm^{-1}$ to optimize the agreement between calculated and measured frequencies of $Si_2H_6$.[9]

Received: November 9, 2012
Published online: December 20, 2012

**Keywords:** Gas-phase chemistry · IR spectroscopy · protonated disilane · silicon · structure elucidation

[1] a) D. M. Smith, P. M. Martineau, P. B. Davies, *J. Chem. Phys.* **1992**, *96*, 1741; b) D. W. Boo, Y. T. Lee, *J. Chem. Phys.* **1995**, *103*, 514; c) Y. B. Cao, J. H. Choi, B. M. Haas, M. S. Johnson, M. Okumura, *J. Phys. Chem.* **1993**, *97*, 5215.

[2] a) J. Fischer, J. Baumgartner, C. Marschner, *Science* **2005**, *310*, 825; b) R. Singh, *J. Phys. Condens. Matter* **2008**, *20*, 045226; c) V. Kumar, Y. Kawazoe, *Phys. Rev. Lett.* **2003**, *90*, 055502; d) R. D. Miller, J. Michl, *Chem. Rev.* **1989**, *89*, 1359.

[3] a) M. C. McCarthy, C. A. Gottlieb, P. Thaddeus, *Mol. Phys.* **2003**, *101*, 697; b) R. I. Kaiser, Y. Osamura, *Astron. Astrophys.* **2005**, *432*, 559.

[4] a) M. J. Kushner, *J. Appl. Phys.* **1988**, *63*, 2532; b) M. L. Mandich, W. D. Reents, M. F. Jarrold, *J. Chem. Phys.* **1988**, *88*, 1703.

[5] a) K. Raghavachari, *J. Chem. Phys.* **1990**, *92*, 452; b) L. A. Curtiss, K. Raghavachari, P. W. Deutsch, J. A. Pople, *J. Chem. Phys.* **1991**, *95*, 2433.

[6] K. Hiraoka, J. Katsuragawa, A. Minamitsu, *Chem. Phys. Lett.* **1997**, *267*, 580.

[7] L. I. Yeh, M. Okumura, J. D. Myers, J. M. Price, Y. T. Lee, *J. Chem. Phys.* **1989**, *91*, 7319.

[8] a) G. E. Douberly, A. M. Ricks, B. W. Ticknor, P. V. R. Schleyer, M. A. Duncan, *J. Am. Chem. Soc.* **2007**, *129*, 13782; b) G. E. Douberly, A. M. Ricks, P. V. R. Schleyer, M. A. Duncan, *J. Chem. Phys.* **2008**, *128*, 021102; c) A. M. Ricks, G. E. Douberly, P. V. R. Schleyer, M. A. Duncan, *Chem. Phys. Lett.* **2009**, *480*, 17; d) A. M. Ricks, G. E. Douberly, P. V. Schleyer, M. A. Duncan, *J. Chem. Phys.* **2010**, *132*, 051101; e) H. S. Andrei, N. Solca, O. Dopfer, *Angew. Chem.* **2008**, *120*, 401; *Angew. Chem. Int. Ed.* **2008**, *47*, 395; f) O. Dopfer, D. Roth, J. P. Maier, *J. Am. Chem. Soc.* **2002**, *124*, 494; g) H. S. Andrei, S. A. Nizkorodov, O. Dopfer, *Angew. Chem.* **2007**, *119*, 4838; *Angew. Chem. Int. Ed.* **2007**, *46*, 4754; h) A. Patzer, S. Chakraborty, N. Solca, O. Dopfer, *Angew. Chem.* **2010**, *122*, 10343; *Angew. Chem. Int. Ed.* **2010**, *49*, 10145; i) N. Solcà, O. Dopfer, *Angew. Chem.* **2002**, *114*, 3781; *Angew. Chem. Int. Ed.* **2002**, *41*, 3628; j) A. Patzer, M. Schütz, T. Möller, O. Dopfer, *Angew. Chem.* **2012**, *124*, 5009; *Angew. Chem. Int. Ed.* **2012**, *51*, 4925; k) M.-E. Crestoni, S. Fornarini, *Angew. Chem.* **2012**, *124*, 7487; *Angew. Chem. Int. Ed.* **2012**, *51*, 7373.

[9] M. Savoca, M. A. R. George, J. Langer, O. Dopfer, *Phys. Chem. Chem. Phys.*, DOI: 10.1039/c2cp43773b.

[10] The NBO charges for the proton in the symmetric X–H–X bonds are −0.42, +0.46, and +0.58 e in $[H_3Si{-}H{-}SiH_3]^+$, $[H_3N{-}H{-}NH_3]^+$, and $[H_2O{-}H{-}OH_2]^+$.

[11] a) R. L. Dekock, W. B. Bosma, *J. Chem. Educ.* **1988**, *65*, 194; b) J. E. McMurry, T. Lectka, *Acc. Chem. Res.* **1992**, *25*, 47.

[12] E. P. L. Hunter, S. G. Lias, *J. Phys. Chem. Ref. Data* **1998**, *27*, 413.

[13] a) G. N. Patwari, T. Ebata, N. Mikami, *J. Chem. Phys.* **2000**, *113*, 9885; b) R. Custelcean, J. E. Jackson, *Chem. Rev.* **2001**, *101*, 1963.

[14] a) G. W. Bethke, M. K. Wilson, *J. Chem. Phys.* **1957**, *26*, 1107; b) J. R. Durig, J. S. Church, *J. Chem. Phys.* **1980**, *73*, 4784; c) N. Moazzen-Ahmadi, V. M. Horneman, *J. Chem. Phys.* **2006**, *124*, 194309.

[15] a) O. Vendrell, F. Gatti, H. D. Meyer, *Angew. Chem.* **2009**, *121*, 358; *Angew. Chem. Int. Ed.* **2009**, *48*, 352; b) S. D. Ivanov, O. Asvany, A. Witt, E. Hugo, G. Mathias, B. Redlich, D. Marx, S. Schlemmer, *Nat. Chem.* **2010**, *2*, 298; c) K. R. Asmis, Y. G. Yang, G. Santambrogio, M. Brummer, J. R. Roscioli, L. R. McCunn, M. A. Johnson, O. Kuhn, *Angew. Chem.* **2007**, *119*, 8846; *Angew. Chem. Int. Ed.* **2007**, *46*, 8691.

[16] a) O. Dopfer, *Int. Rev. Phys. Chem.* **2003**, *22*, 437; b) O. Dopfer, *Z. Phys. Chem.* **2005**, *219*, 125; c) E. J. Bieske, O. Dopfer, *Chem. Rev.* **2000**, *100*, 3963.

[17] M. J. Frisch, G. W. Trucks, H. B. Schlegel, G. E. Scuseria, M. A. Robb, J. R. Cheeseman, G. Scalmani, V. Barone, B. Mennucci, G. A. Petersson, H. Nakatsuji, M. Caricato, X. Li, H. P. Hratchian, A. F. Izmaylov, J. Bloino, G. Zheng, J. L. Sonnenberg, M. Hada, M. Ehara, K. Toyota, R. Fukuda, J. Hasegawa, M. Ishida, T. Nakajima, Y. Honda, O. Kitao, H. Nakai, T. Vreven, J. A. Montgomery Jr., J. E. Peralta, F. Ogliaro, M. Bearpark, J. J. Heyd, E. Brothers, K. N. Kudin, V. N. Staroverov, R. Kobayashi, J. Normand, K. Raghavachari, A. Rendell, J. C. Burant, S. S. Iyengar, J. Tomasi, M. Cossi, N. Rega, N. J. Millam, M. Klene, J. E. Knox, J. B. Cross, V. Bakken, C. Adamo, J. Jaramillo, R. Gomperts, R. E. Stratmann, O. Yazyev, A. J. Austin, R. Cammi, C. Pomelli, J. W. Ochterski, R. L. Martin, K. Morokuma, V. G. Zakrzewski, G. A. Voth, P. Salvador, J. J. Dannenberg, S. Dapprich, A. D. Daniels, Ö. Farkas, J. B. Foresman, J. V. Ortiz, J. Cioslowski, D. J. Fox, Gaussian 09 Rev. A.02, Gaussian Inc., Wallingford CT, **2009**..

  